# Effects of laser peening on the fatigue strength and defect tolerance of aluminum alloy

Koji Takahashi[1], Yuta Kogishi[1], Norihito Shibuya[2], Fumiaki Kumeno[2]

[1]Yokohama National University, 79-5 Tokiwadai, Hodogaya, Yokohama, Japan

[2]Sintokogio, LTD, 180-1, Komaki, Ohgi-cho, Toyokawa, Aichi, Japan

*Correspondence*:

Dr. Koji Takahashi

Professor, Faculty of Engineering

Yokohama National University

79–5, Tokiwadai, Hodogaya, Yokohama, 240–8501, Japan

## Abstract

The effects of laser peening (LP) on the bending fatigue strength of the 7075–T651 aluminum alloy were investigated. Accordingly, the defect tolerance of the aluminum alloy subjected to LP is discussed based on fracture mechanics. The results indicate that a deeper compressive residual stress was induced by LP compared with the case of shot peening (SP). The fatigue strengths increased when both peening types were used. Semicircular slits with depths less than 0.4 and 0.1 mm were rendered harmless based on the applications of LP and SP, respectively. The apparent threshold stress intensity factor range $\Delta K_{th,ap}$ increased by approximately five and two times owing to LP and SP, respectively. The increase of the $\Delta K_{th,ap}$ was caused by the compressive residual stress induced by the peening. The Kitagawa–Takahashi diagram of the laser peened specimens shows that the defect tolerance of the aluminum alloy was improved by LP.

**KEYWORDS**

Laser peening, Shot peening, Fatigue strength, Residual stress, Aluminum alloy, Defect tolerance

**NOMENCLATURE**

$a$ depth of slit

$a_{max}$ maximum slit size rendered harmless by peening

$a_0$ intrinsic defect size

$A_p$ spot area

$C_v$ coverage

$\Delta\sigma$ stress range

$\Delta\sigma_w$ fatigue strength after $10^7$ cycles

$\Delta\sigma_{w0}$ fatigue strength of the as-machined (AM) specimens after $10^7$ cycles

$\Delta K_{th}$ threshold stress intensity factor range

$\Delta K_{th,ap}$ apparent threshold stress intensity factor range

$D$ spot diameter of the laser

$E_p$ pulse energy

$F$ shape factor of surface cracks

$G$ power density

$N_f$ number of cycles to failure

$N_p$ irradiation density

$R$ stress ratio

$R_a$ arithmetic mean roughness

$t$ pulse duration

## 1. INTRODUCTION

Owing to its high-specific strength, the uses of aluminum alloys in transportation equipment is expanding. Improvement of the fatigue strengths of aluminum alloys can contribute to the increase of the reliability of the transportation equipment. Laser peening (LP) is a surface modification technology that introduces compressive residual stress to the surface of materials based on the utilization of local impact action generated by the irradiation of short laser pulses[1]. The effects of LP on the fatigue strength of aluminum alloys have been reported previously[2–9]. The depth of compressive residual stress induced by laser peening is deeper than that by conventional shot peening (SP). This is attributed to an enhanced fatigue strength compared to that in the case of conventional shot peening[2–4,8,9].

Surface defects, such as scratches, cracks, and corrosion pits, decrease the fatigue strength of aluminum alloy components[10–13]. Thus, nondestructive inspections are periodically carried out to maintain the structural integrity of these components. However, there is a danger of overlooking the defect after this type of inspection. If the surface defects can be rendered harmless from the viewpoint of the fatigue strength based on a thorough peening treatment, the reliability of the components can be improved. Takahashi and co-authors clarified that the fatigue strength of spring steel specimens with artificial surface defects could be improved with SP by the same level as that attained in the cases of defect-free steel specimens subjected to the same SP[14,15]. Similar effects of SP and needle peening have been reported in various other materials for the rendering of harmless surface defects[16–18]. Specifically, Takahashi et al. clarified that semicircular slits with depths of 0.1 mm in the aluminum alloy A7075–T651 could be rendered harmless by performing SP[19]. Several studies have shown that the propagation of fatigue cracks in aluminum alloys are delayed by applying LP at the tip of these cracks[6,20–23]. The effects of LP on metals introduced with artificial defects has also been studied [24-26]. Smyth et al. applied LP to A2024-T351 containing scratch defects and reported that fatigue crack growth was suppressed and fatigue life extended by LP[24]. They successfully predicted fatigue life after LP based on fracture mechanics. It was also reported that LP was effective in improving fatigue strength of Ti-6Al-4V containing surface defects induced by foreign objective damage[25, 26]. However, the maximum surface defect size that can be rendered harmless by LP has not yet been studied.

The objective of this study is to clarify the maximum defect size rendered harmless by LP based on the fatigue strength of aluminum alloy. A semicircular slit was introduced on the surface of aluminum alloy specimens which were subjected to LP. Bending fatigue tests were then carried out to evaluate the fatigue strength. The effects of LP on the defect tolerance of aluminum were investigated based on fracture mechanics. The experimental results were compared with the case of SP. As the result, it was clarified that large surface defects could be rendered harmless when LP was used in comparison with SP.

## 2. EXPERIMENTS

### 2.1 Materials and specimens

High-strength aluminum alloy A7075–T651 was used as the test material. The 0.2% proof stress of the as-machined material was 505 MPa and its tensile strength was 570 MPa. Fatigue test specimens with a thickness of 4 mm were machined. Figure 1(A) shows the shapes and dimensions of the bending fatigue test specimens.

Figure 2 shows the flowchart of the machining process of the bending fatigue test specimens. The tested specimens were classified into six groups: as-machined specimens (AM), AM specimens treated with laser peening (AM+LP), AM specimens treated with shot peening (AM+SP), AM specimens with a semicircular slit (AM+Slit), LP treated specimens with a semicircular slit (LP+Slit), and SP treated specimens with a semicircular slit (SP+Slit).

Figure 1(B) shows the shape and dimension of the semicircular slit. A semicircular slit was introduced into the smallest cross-section of the specimen with electric discharge machining to emulate a crack-like surface defect. The direction of the semicircular slit was perpendicular to the longitudinal direction. The depths of the semicircular slits were $a$ = 0.1–0.6 mm for the AM+Slit specimens, $a$ = 0.4 and 0.6 mm for the LP+Slit specimens, and $a$ = 0.1 and 0.2 mm for the SP+Slit specimens. The widths of the slits were approximately 0.03 mm. In the cases of the LP+Slit and SP+Slit specimens, a semicircular slit was introduced after LP treatment to avoid peening inside the slit.

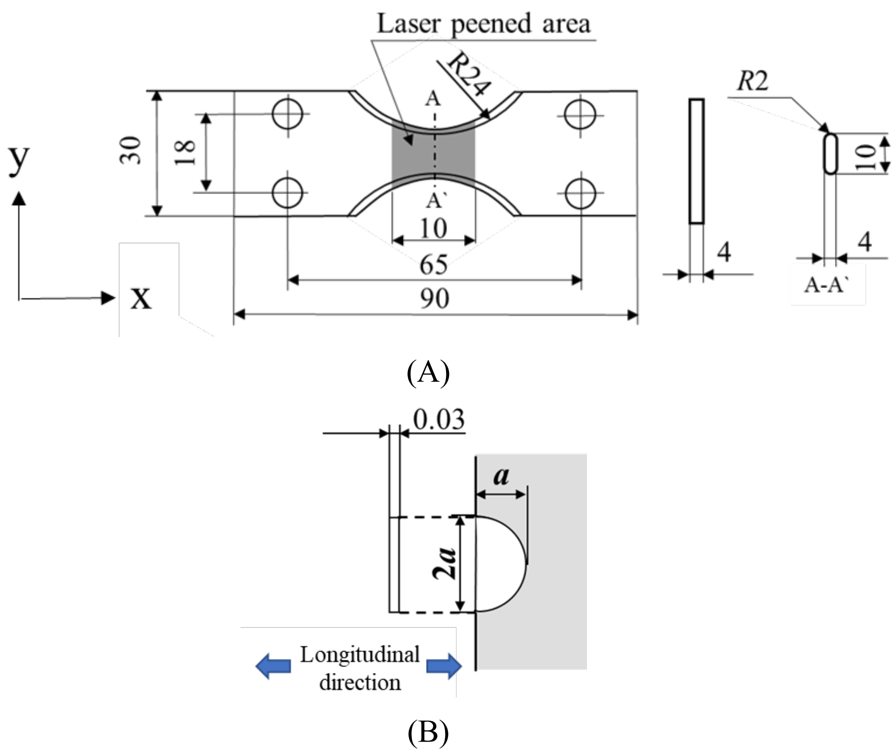


FIGURE 1 Shapes and dimensions of (A) bending fatigue test specimen, and (B) semicircular slit (unit: mm)

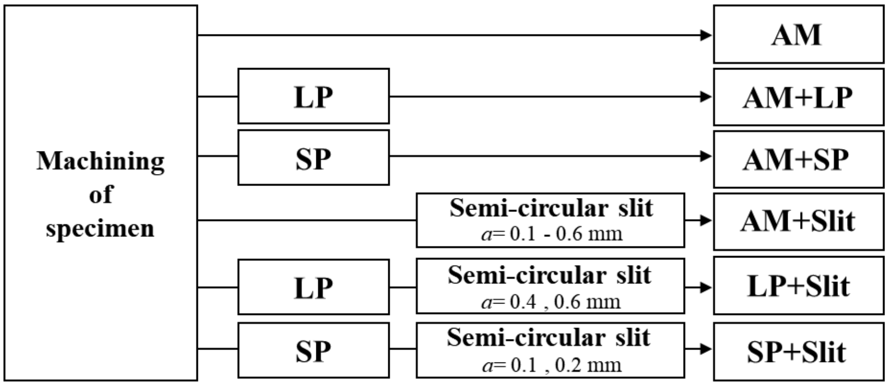


FIGURE 2 Flowchart of the machining process of tested specimens

## 2.2 Laser peening conditions

Laser peening was performed on AM specimens in water. Figure 3(A) shows the setup of the laser peening device. Coating was not used on the surface of the specimens. The second harmonic of Q-switched Nd: YAG laser was used. The laser peening condition is listed in Table 1(A). This condition was selected based on the study by Masaki et al.[27]. Figure 3(B) shows the tracked laser in the laser peened area. The spot diameter ($D$) is the diameter of each laser spot. The pulse energy ($E_p$) indicates the energy contained per laser pulse. Additionally, the irradiation density ($N_p$) indicates the number of pulses irradiated per unit area. The pulse interval (overlapping pitch) was 0.134 mm, as shown in Figure 3(B). Thus, the laser was irradiated at 7.46 (pulse/mm) per unit length. We then obtained $N_p = 56$ (pulse/mm$^2$) per unit area. The power density $G$ can be calculated by the following equation using the $E_p$, the spot area $A_p$ (= $\pi D^2/4$), and pulse duration ($t$),

$$G = \frac{E_p}{A_p t} \qquad (1)$$

The coverage $C_v$, which is the overlapping amount per unit area, is calculated using the following equation[7] based on the irradiation density $N_p$ and the spot area $A_p$:

$$C_v = N_p A_p \qquad (2)$$

As a result, the power density $G$ = 12 GW/cm$^2$ and the coverage $C_v$ = 700%.

The laser peened area of the specimen is shown in Figure 1(A). It has been reported that the test specimens with thickness of 2 mm warped after LP on one side[24]. In this study, we performed LP on both sides of the test specimens to suppress the wrap. The laser beam was rastered over the specimens in the y (width) direction followed by shifting in the x (longitudinal) direction in one layer (see Figure 3(B)).

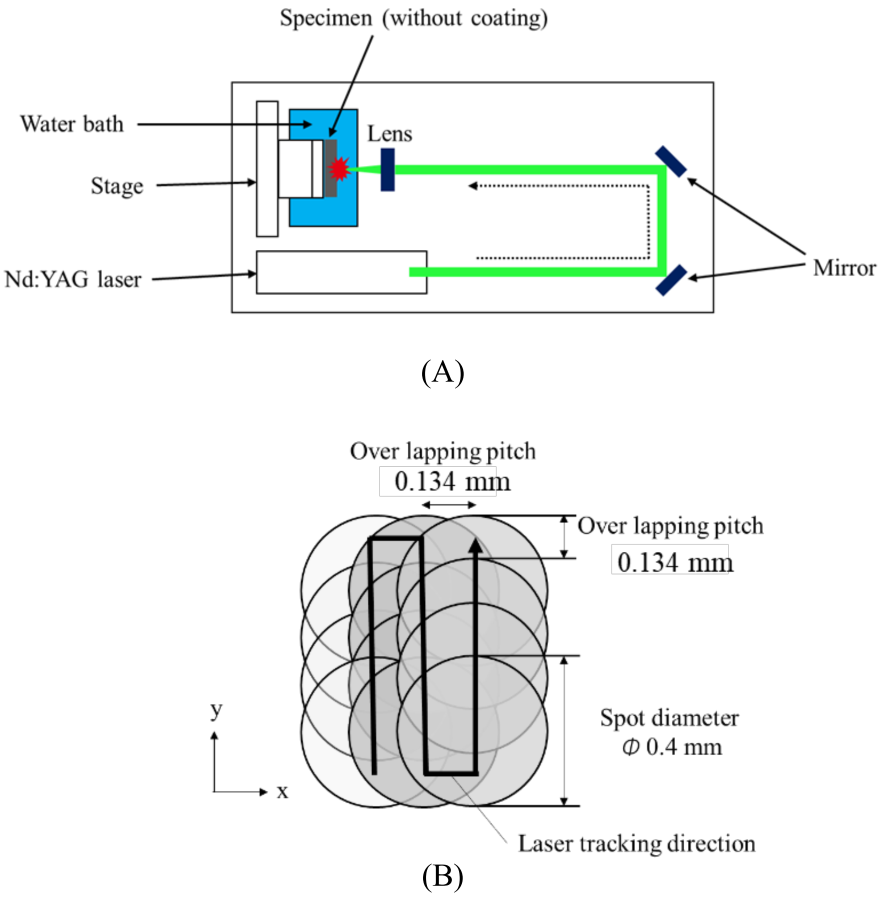


FIGURE 3 Schematic of laser peening procedure: (A) setup of laser peening (LP) device, and (B) laser tracking within the laser peened area

TABLE 1 Peening conditions:(A) laser peening, and (B) shot peening

(A)

| | |
|---|---|
| Spot diameter, *D* | 0.4 mm |
| Pulse duration, *t* | 6.2 ns |
| Pulse energy, $E_p$ | 93 mJ |
| Irradiation density, $N_p$ | 56 pulse/mm$^2$ |
| Power density, *G* | 12 GW/cm$^2$ |
| Coverage, $C_v$ | 700% |

(B)

| | |
|---|---|
| Shot material | $ZrO_2$ |
| Shot hardness | 1330 HV |
| Shot diameter | 300 μm |
| Air pressure | 0.2 MPa |
| Standoff distance | 100 mm |
| Coverage | 300% |
| Arc height | 0.173 mmA |

### 2.3 Shot peening conditions

SP was performed on both sides of AM specimens using a direct pressure peening system. Table 1(B) lists the conditions of SP. In this case, $ZrO_2$ ceramic shots were used with diameters of 300 μm. The peening intensity evaluated with an A-type Almen strip was 0.173 mm.

### 2.4 Measurement of surface roughness, residual stress distribution, and vickers hardness distribution

Arithmetic mean roughness $R_a$ was measured in the longitudinal direction of the specimen using a stylus-type roughness measuring machine. The measurement length was 4 mm and the average values of three data points were compared. The three-dimensional (3D) profiles of the AM, AM+LP, and AM+SP specimens were measured using a laser microscope.

The residual stress from the surface to the depth direction of the test specimen was measured by the cosα method using an X-ray measurement apparatus. Table 2 shows the detailed conditions of the residual stress measurement. Electro-polishing was used to remove different specimen layers. The residual stress in the longitudinal direction at a central part of the surface was successively measured for each layer. Stress redistribution occurred after the removal of the surface. Thus, stress correction calculation[28] was performed for each measured result.

Vickers hardness distributions were measured for the polished cross section of each specimen using a micro Vickers hardness tester. The hardness tests were conducted with a holding time of 15 s and a load of 0.98 N. Three points were measured at each depth and the average value was plotted.

TABLE 2 Residual stress measurement conditions

| | |
|---|---|
| Method | cosα |
| Tube bulb | Cr |
| Measurement surface | (3.1.1) plane |
| Collimator diameter | Φ1.0 mm |
| Voltage value | 30 kV |
| Current value | 1.0 mA |

## 2.5 Fatigue test method

Fatigue tests were performed using a bending fatigue testing machine at a stress ratio $R$ = 0 and a frequency of 20 Hz at temperatures in the range of 23–28 °C in air. The nominal bending stress at the surface of the minimum cross-section of the specimen was also evaluated. Typically, fatigue limits of aluminum alloy could not be defined. Thus, the fatigue strengths were evaluated after $10^7$ cycles. Three to four specimens were used to determine the $10^7$ cycles fatigue strength of each test condition. The minimum step of the stress range $\Delta\sigma$ was set to 20 MPa. After the fatigue tests, the fracture surfaces of the specimens were observed with a scanning electron microscope (SEM).

# 3. EXPERIMENTAL RESULTS

## 3.1 Surface roughness of specimens

The measured values of $R_a$ were 0.146 μm, 2.108 μm, and 2.277 μm for AM, LP, and SP materials, respectively. The surface roughness increased after LP and SP. The values of $R_a$ after LP and SP are almost identical. Figure 4 shows the 3D profiles measured using laser microscopy. Machining scratches were confirmed in the longitudinal direction in the AM specimens (Figure 4(A)). Laser peening eliminated the machining scratches and made ablation marks on the surface because coating was not used in the LP process (Figure 4(B)). In SP specimens, shot peening also eliminated the machining scratches and made crater-like dents on the surface (Figure 4(C)). The dents were caused by the impact of shots. These surface irregularities increased the surface roughness.

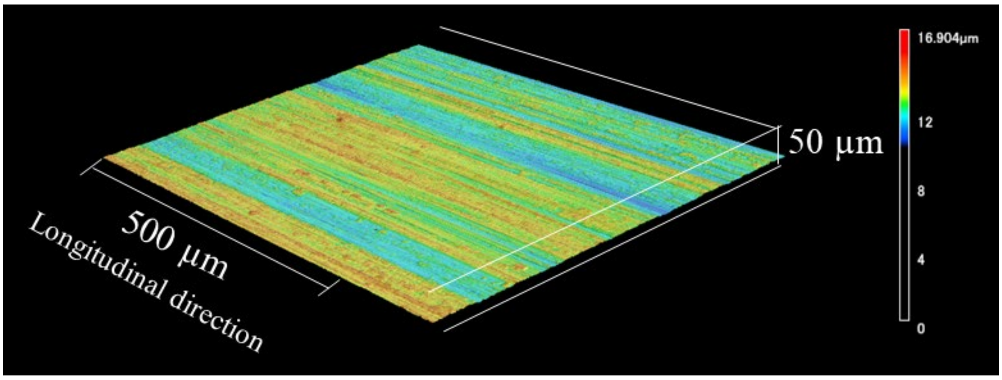


(A)

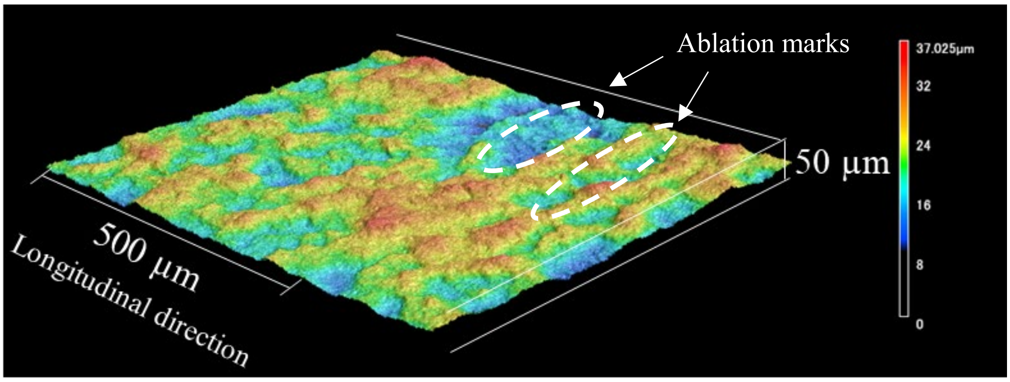


(B)

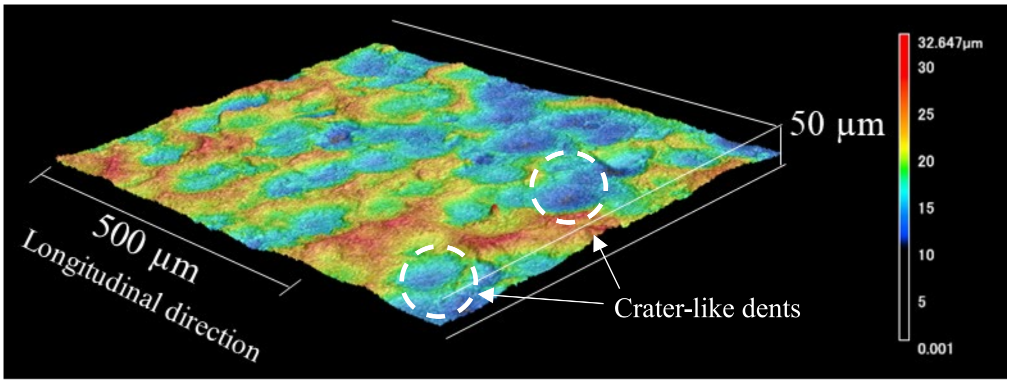


(C)

FIGURE 4 Three-dimensional (3D) profiles of tested specimens: (A) As-machined specimen, (B) LP specimen, and (C) shot peened (SP) specimen

### 3.2 Residual stress distributions

Figure 5 shows the residual stress distribution for the laser peened specimens. Normal stresses in the longitudinal direction were measured. For comparison, the residual stress distributions for the AM (non-peening) and SP specimens are also indicated. A compressive residual stress of 50 MPa was induced by machining and is measured in the AM specimens. The surface compressive residual stress of the LP specimens was 295 MPa, and the depth of the compressive residual stress is 0.7 mm. The residual stress value of the surface of SP specimens was 211 MPa, and the depth of compressive residual stress was 0.2 mm. Thus, the compressive residual stress at the surface of the LP specimen was larger than that of the SP specimen. Moreover, a deep compressive residual stress was introduced by LP as compared to that of the SP.

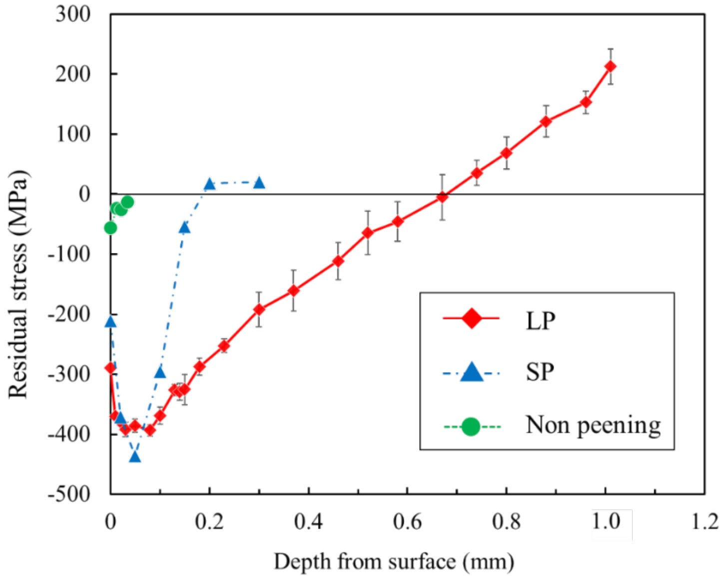


FIGURE 5 Distributions of residual stress in the longitudinal direction

### 3.3 Vickers hardness distribution

Figure 6 shows the Vickers hardness distribution measured on the cross section of each specimen. The average hardness distribution was obtained from three measurements of the hardness at each depth. Compared with the AM specimen, the hardness values of the LP and SP specimens increased. The increase in the rate of hardness showed the same trends as the residual stress distribution.

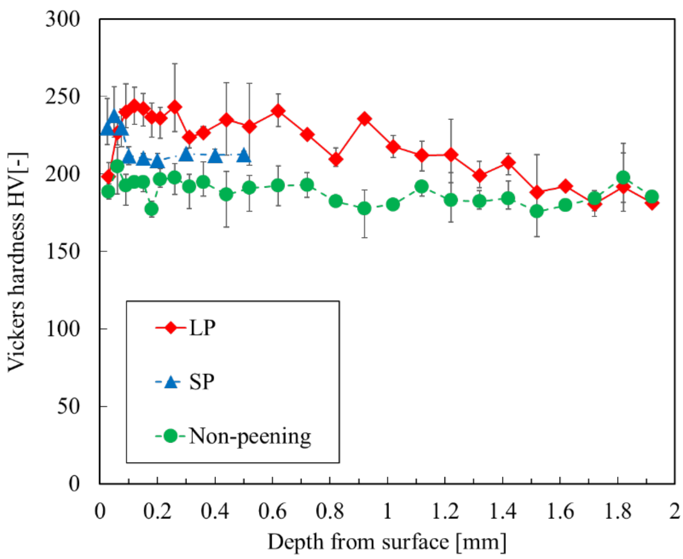


FIGURE 6 Distributions of Vickers hardness at the section of each specimen

### 3.4 Effects of LP and SP on fatigue strength

Figure 7 shows the relationship between the stress range Δσ and the slit depth $a$. The solid symbols indicate the fractured specimens during the fatigue tests. The open symbols represent the specimens that did not fracture after $10^7$ cycles. The maximum value of Δσ among the nonfractured specimens corresponds to the fatigue strength after $10^7$ cycles $\Delta\sigma_w$.

The fatigue strength of the AM specimens ($\Delta\sigma_{w0}$) after $10^7$ cycles respectively increased by 27% and 7% after the LP and SP treatments. This result is discussed in section 4.1. The figure outcomes demonstrate that the fatigue strengths of the nonpeened specimens decrease when the slit depth increases. However, both peening types increase the fatigue strength. The $\Delta\sigma_w$ values of the specimens with slit depths $a$ = 0.1 mm and 0.2 mm increased by 100% with SP treatment. The $\Delta\sigma_w$ of the specimens with a slit depth $a$ = 0.4 mm and 0.6 mm increased by 400% and 433% with the use of the LP treatment. Thus, LP is more effective than SP in increasing the fatigue strengths owing to the large and deep compressive residual stress induced by LP.

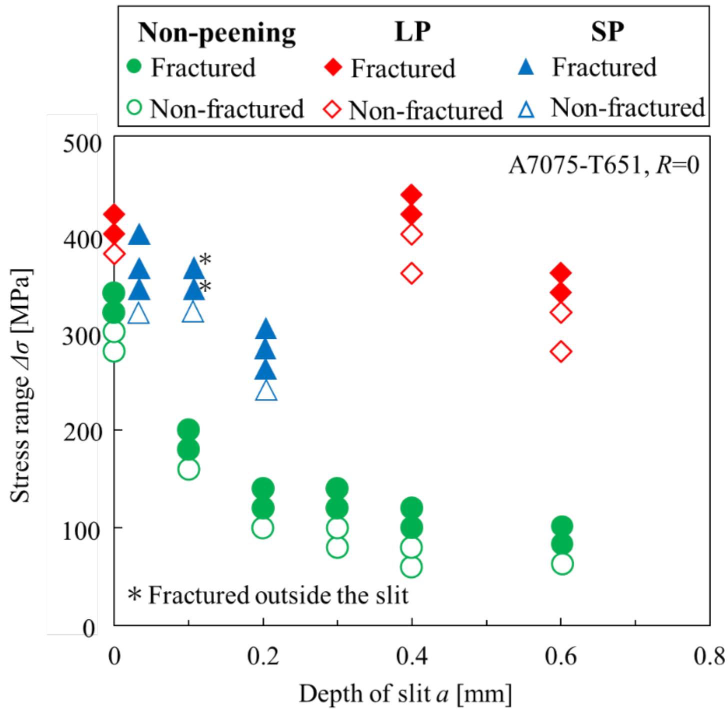


FIGURE 7 Fatigue test results on nonpeened, LP, and SP specimens

### 3.5 Fracture surface observation results

Figure 8 shows the fracture surfaces of the AM, AM+LP, and AM+SP specimens. Crack initiation sites were found to be sub-surface in all of the AM, AM+LP, and AM+SP specimens. This is because the compressive residual stress was induced on the surfaces of these specimens (see Figure 5). The fatigue cracks were initiated mostly due to cleavage-like matrix cracking. This type of cracking is often observed when fatigue crack propagate in aluminum alloys after an initial crack occurs at the interior of specimen[12,19,27]. The depths of the crack initiation sites of the AM+LP specimens were much deeper than those of the AM and AM+SP specimens. This behavior can be attributed to the deeper compressive residual stress of the LP treatment because the fatigue crack propagation behavior was affected by the compressive residual stress[8].

Figure 9 shows the fracture surfaces of the AM+Slit specimens. The fatigue crack initiation sites for these specimens were identified at the slits. The fatigue cracks were initiated uniformly at the front of the semicircular slit and propagated along a semicircular trajectory.

Figure 10(A) and (B) shows the fracture surfaces of the LP+Slit specimens. The fatigue crack initiation sites for these specimens were also identified at the slits. The fatigue cracks were initiated at the deepest point of the semicircular slit and propagated along a complicated trajectory owing to the effects of compressive residual stress.

Figure 10(C) and (D) shows the fracture surfaces of the SP+Slit specimens. Specimens with a 0.1 mm slit fractured outside the slit (Figure 10(C)). This is probably because the slit depth was as small as 0.1 mm, and specimens fractured from matrix cracking similar to AM+SP specimens.

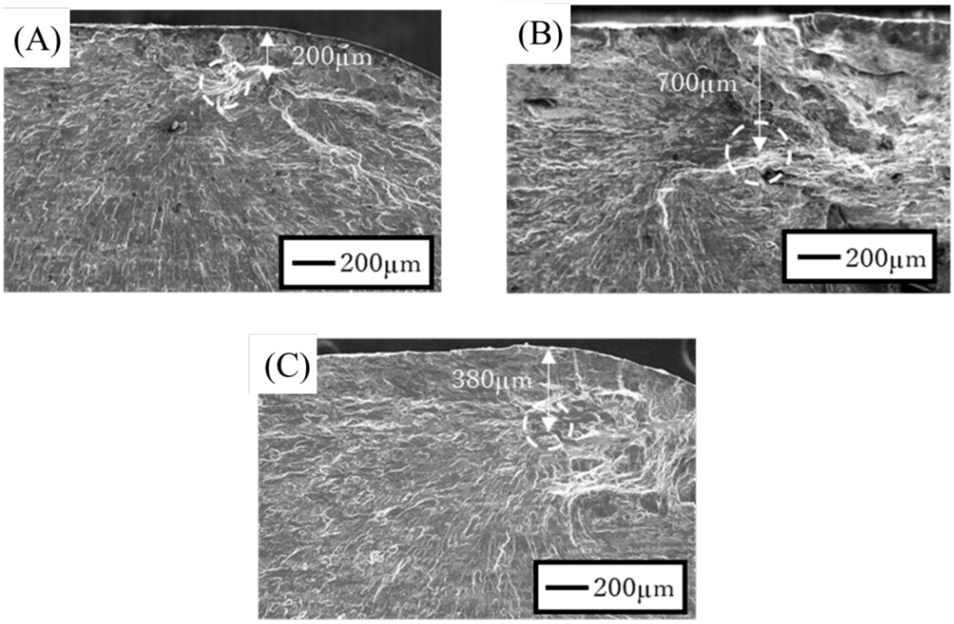


FIGURE 8 Scanning electron microscopy (SEM) images of fractured surfaces: (A) AM, (B) AM+LP, and (C) AM+SP

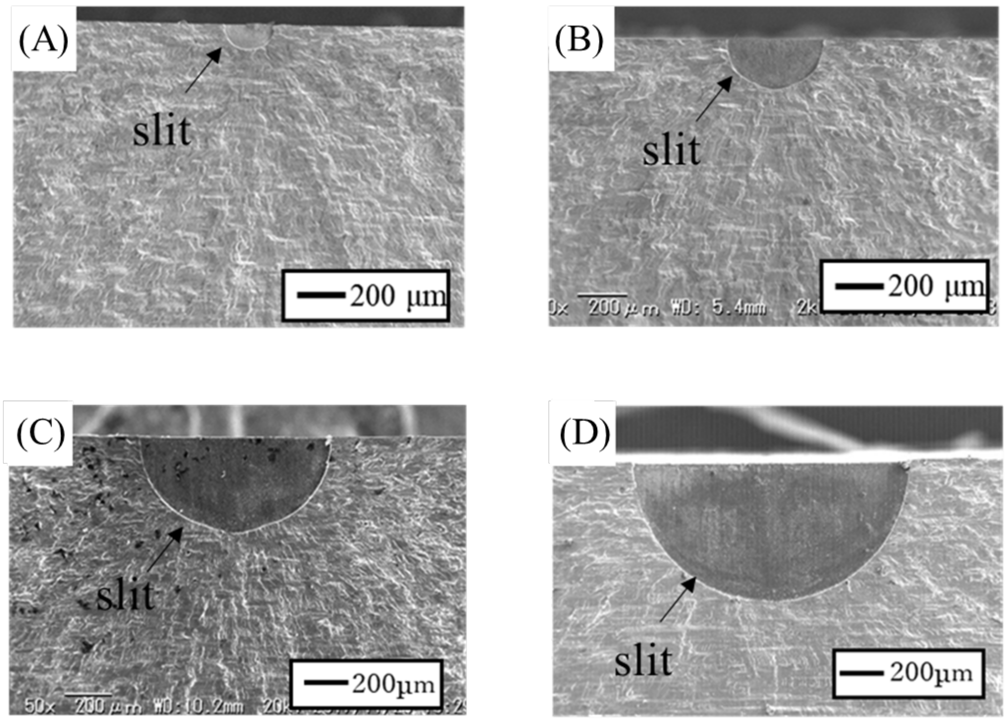


FIGURE 9 SEM images of fractured surface of AM+Slit: (A) $a$ = 0.1 mm, (B) $a$ = 0.2 mm, (C) $a$ = 0.4 mm, and (D) $a$ = 0.6 mm

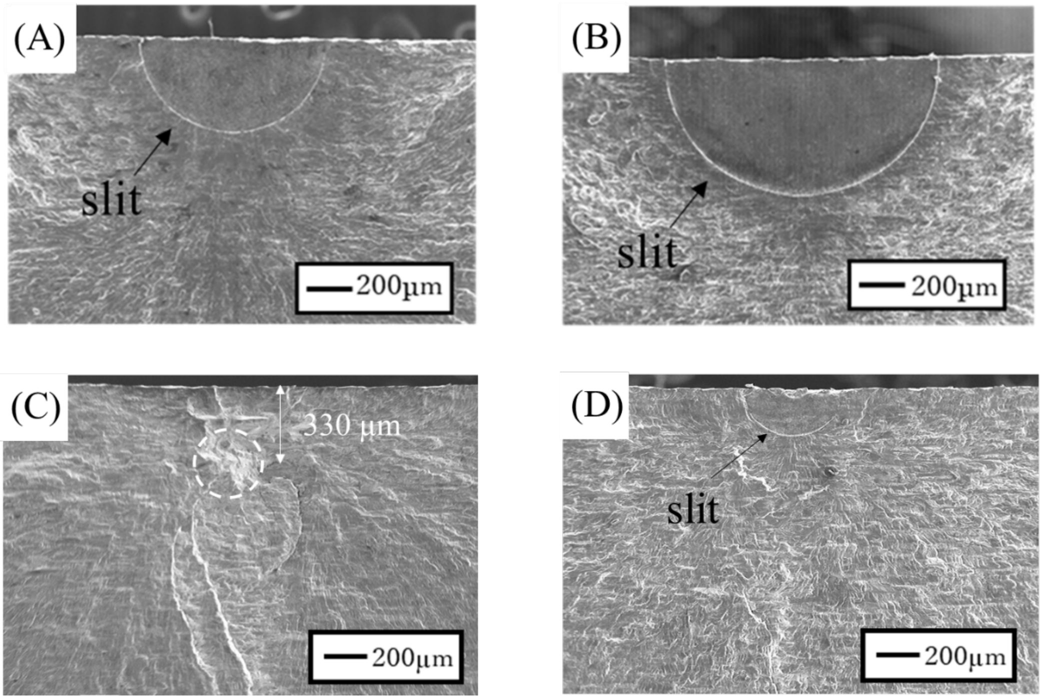


FIGURE 10 SEM images of fractured surface: (A) LP+Slit $a$ = 0.4 mm, (B) LP+Slit $a$ = 0.6 mm, (C) SP+Slit $a$ = 0.1 mm, and (D) SP+Slit $a$ = 0.2 mm

### 3.6 Maximum defect size that can be rendered harmless

The conditions used in this experiment to render the slit harmless were defined based on our previous studies[29] as follows: (a) the $\Delta\sigma_w$ value increased by more than 95% compared to the $\Delta\sigma_{w0}$ value for the AM+LP (AM+SP) or (b) more than half the specimens fractured outside the slit.

As shown in Figure 7, in the case of $a$ = 0.4 mm, the $\Delta\sigma_w$ value of LP+Slit specimens was 400 MPa and >95% of $\Delta\sigma_{w0}$ for AM+LP specimens (380 MPa). Conversely, in the case of $a$ = 0.6 mm, the $\Delta\sigma_w$ value of LP+Slit specimens was 320 MPa. From these results, it is revealed that the maximum defect size that can be rendered harmless by LP is $a_{max}$ = 0.4 mm. As the SP+Slit specimen with $a$ = 0.1 mm slit satisfies both (a) and (b), the maximum defect size that can be rendered harmless by SP is determined to be $a_{max}$ = 0.1 mm. Therefore, larger surface defects could be rendered harmless by applying LP compared with SP.

# 4. DISCUSSION

## 4.1 Effects of residual stress, hardness, and surface roughness on fatigue strength

The fatigue strength of the AM specimens ($\Delta\sigma_{w0}$) after $10^7$ cycles increased by 27% and 7%, respectively, after the LP and SP treatments (see section 3.4). Here, the effects of LP and SP on $\Delta\sigma_{w0}$ are discussed in terms of residual stress, hardness, and surface roughness.

As mentioned in Section 3.2, the compressive residual stress at the surface of the LP specimen is larger than that of the SP specimen. The compressive residual stress was deeper for LP compared to SP. Thus, fatigue crack growth in the laser peened specimens could be hindered more effectively than it could in shot peened specimens. As a result, the depth of the fatigue crack initiation site of the former was much deeper than that of the latter, as noted in section 3.5. The values of *HV* at the sub-surface in the laser peened specimens were larger than those of the shot peened specimens. Thus, the fatigue strength of the LP specimen is larger than that of the SP specimen.

Next the effects of surface roughness are discussed. As mentioned in section 3.1, surface roughness increased after LP and SP. The fatigue crack initiation sites for the AM+LP and AM+SP specimens were sub-surface. Thus, the surface roughness did not affect the fatigue strength in this study. However, if the surface roughness increased due to peening, the roughness could affect fatigue strength.

## 4.2 Effects of LP and SP on the defect tolerance

The effects of LP on the defect tolerance of aluminum alloys were investigated. First, we compared the apparent threshold stress intensity factor ranges $\Delta K_{th,ap}$ for each specimen. The values of $\Delta K_{th,ap}$ were calculated based on the following equation.

$$\Delta K_{\mathrm{th,ap}} = F\Delta\sigma_w\sqrt{\pi a} \quad \cdots (3)$$

where $F$ indicates the shape factor of the surface crack which was calculated using the Newman–Raju's equation[30]. The $\Delta K_{th,ap}$ is different from intrinsic threshold stress intensity factor range ($\Delta K_{th}$), which is a material property. Table 3 lists the values of $\Delta K_{th,ap}$ calculated based on the $\Delta\sigma_w$ values of each specimen. Figure 11 shows the relationship between the $\Delta K_{th,ap}$ and the depth of slit $a$. It is noted in Figure 11 that the values of $\Delta K_{th,ap}$ were almost constant for each specimen. The average value of $\Delta K_{th,ap}$ for nonpeened specimens matches $\Delta K_{th}$ obtained from several experimental results for similar materials[31,32]. It was revealed that the $\Delta K_{th,ap}$ increased by approximately two times with SP and by five times with LP. The increase of the $\Delta K_{th,ap}$ was caused by the retardation of the crack propagation owing to the compressive residual stress. The values of $\Delta K_{th,ap}$ for nitrided steel[33] and copper alloy[34] specimens with microholes were increased by at most two times after SP. Thus, the LP is more effective in increasing the value of $\Delta K_{th,ap}$ compared to SP.

Figure 12 shows the Kitagawa–Takahashi diagram[35] which plots the relationship between $\Delta\sigma_w$ and the crack (slit) depth. Many equations have been proposed to model the Kitagawa–Takahashi diagram. Among them, Smith's model[36] was used for its simplicity. In the Smith model, the relationship between $\Delta\sigma_w$ and crack depth is expressed by two straight lines[37]. The horizontal straight lines show the $\Delta\sigma_{w0}$ values for the AM, AM+SP, and AM+LP specimens. The lines with slopes equal to −1/2 indicate the calculated values of $\Delta\sigma_w$ based on the substitution of the average values of $\Delta K_{\text{th,ap}}$ in the following equation.

$$\Delta\sigma_w = \frac{\Delta K_{\text{th,ap}}}{F\sqrt{\pi a}} \quad \cdot\cdot\cdot (4)$$

The values of the fictitious intrinsic defect size ($a_0$), which is the intersection of the two straight lines of Smith's model, were calculated by the following equation[38].

$$a_0 = \frac{1}{\pi}\left(\frac{\Delta K_{\text{th,ap}}}{\alpha \Delta\sigma_{w0}}\right)^2 \quad \cdot\cdot\cdot (5)$$

It can be observed from Figure 12 that the Smith's model can estimate the fatigue strength with higher accuracy. The calculated values of $a_0$ were 0.03 mm for nonpeening, 0.10 mm for SP, and 0.40 mm for LP. It is noted that the value of $a_0$ is close to the experimental results of $a_{max}$ which were obtained in this study. These analytical results demonstrated that the defect tolerance of the aluminum alloy was increased with LP.

TABLE 3 The values of $\Delta K_{\text{th,ap}}$ for each specimen

| Specimen | $a$ [mm] | $\Delta\sigma_w$ [MPa] | $\Delta K_{\text{th,ap}}$ [MPa·m$^{1/2}$] |
|---|---|---|---|
| AM+Slit | 0.1 | 160 | 2.04 |
| | 0.2 | 100 | 1.79 |
| | 0.3 | 100 | 2.16 |
| | 0.4 | 80 | 1.99 |
| | 0.6 | 60 | 1.79 |
| LP+Slit | 0.4 | 400 | 9.92 |
| | 0.6 | 320 | 9.56 |
| SP+Slit | 0.1 | 320 | 4.09 |
| | 0.2 | 200 | 3.93 |

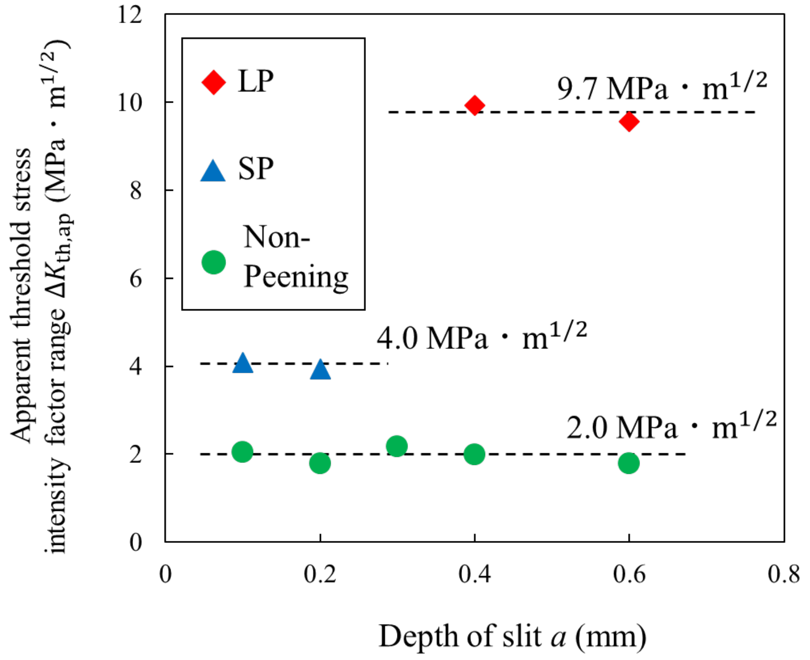


FIGURE 11 Relationship between $\Delta K_{\mathrm{th,ap}}$ and depth of slit

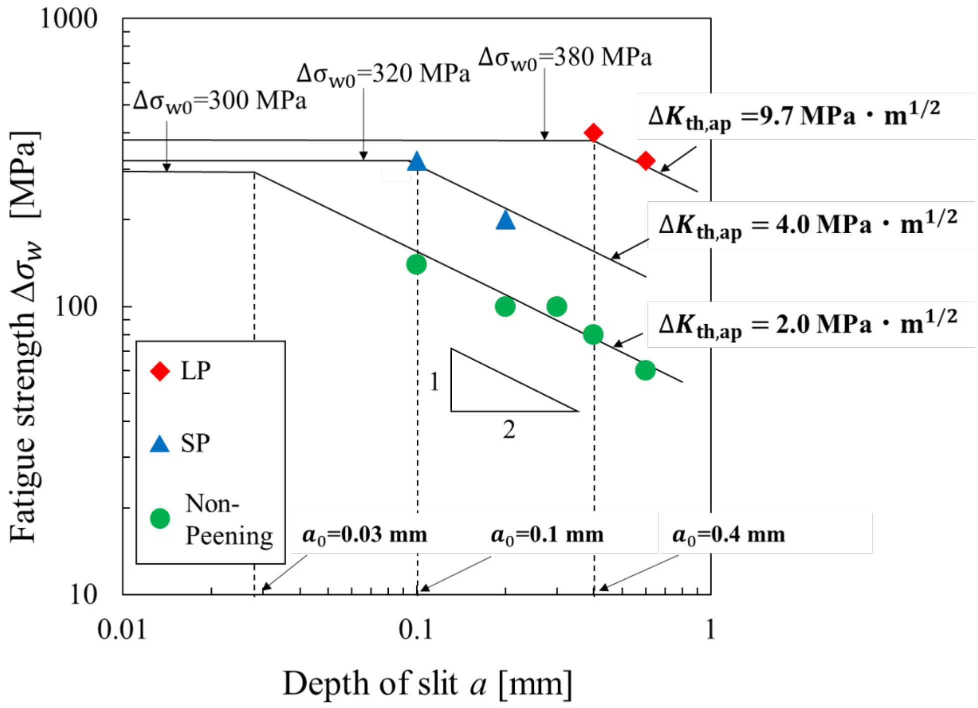


FIGURE 12 Relationship between $\Delta\sigma_{\mathrm{w}}$ and depth of slit

## 5. CONCLUSIONS

In this study, we investigated the effects of LP on the fatigue strength of the aluminum alloy A7075–T651 which contained crack-like surface defects. The effects of LP on the defect tolerance of the aluminum alloy were investigated based on fracture mechanics. The evoked results can be summarized as follows.

1. By performing LP, a compressive residual stress can be introduced at the depth of 0.7 mm from the surface. Thus, a deep compressive residual stress was induced compared with the case of SP (0.2 mm).
2. The maximum defect size that can be rendered harmless by LP was 0.4 mm, which was much larger than that induced by SP (0.1 mm). Thus, larger surface defects could be rendered harmless by applying LP compared with SP.
3. The apparent values of threshold stress intensity factor range ($\Delta K_{th,ap}$) increased by approximately two times when SP was used and by five times when LP was used. The increases of the $\Delta K_{th,ap}$ values were caused by the compressive residual stress which was induced by LP.
4. The Kitagawa–Takahashi diagram of the LP specimens showed that the defect tolerance of the aluminum alloy increased when LP was performed.

## TABLES

TABLE 1 Peening conditions:(A) laser peening, and (B) shot peening

TABLE 2 Residual stress measurement conditions

TABLE 3 The values of $\Delta K_{th,ap}$ for each specimen

**FIGURES**

FIGURE 1 Shapes and dimensions of (A) bending fatigue test specimen and (B) semicircular slit (unit: mm)

FIGURE 2 Flowchart of the machining process of tested specimens

FIGURE 3 Schematic of laser peening procedure: (A) setup of laser peening (LP) device, (B) laser tracking within the laser peened area

FIGURE 4 Three-dimensional (3D) profiles of tested specimens: (A) As-machined specimen, (B) LP specimen, and (C) shot peened (SP) specimen

FIGURE 5 Distributions of residual stress in the longitudinal direction

FIGURE 6 Distributions of Vickers hardness at the section of each specimen

FIGURE 7 Fatigue test results on nonpeened, LP, and SP specimens

FIGURE 8 Scanning electron microscopy (SEM) images of fractured surfaces: (A) AM, (B) AM+LP, and (C) AM+SP

FIGURE 9 SEM images of fractured surface of AM+Slit: (A) a = 0.1 mm, (B) a = 0.2 mm, (C) a = 0.4 mm, and (d) a = 0.6 mm

FIGURE 10 SEM images of fractured surface: (A) LP+Slit $a$ = 0.4 mm, (B) LP+Slit $a$ = 0.6mm, (C) SP+Slit $a$ = 0.1 mm, and (D) SP+Slit $a$ = 0.2 mm

FIGURE 11 Relationship between $\Delta K_{th,ap}$ and depth of slit

FIGURE 12 Relationship between $\Delta\sigma_w$ and depth of slit

**REFERENCES**

1. Fairand BP, Wilcox BA, Gallagher WJ, Williams DN. Laser shock‐induced

microstructural and mechanical property changes in 7075 aluminum. *J Appl Phys.* 1972;43(9): 3893–3895.

2. Peyre P, Fabbro R, Merrien P, Lieurade HP. Laser shock processing of aluminium alloys. Application to high cycle fatigue behaviour. *Mater Sci Eng: A.* 1996;210(1): 102–113.

3. Rodopoulos CA, Romero JS, Curtis SA, de los Rios ER, Peyre P. Effect of controlled shot peening and laser shock peening on the fatigue performance of 2024-T351 aluminum alloy. *J Mater Eng Perform.* 2003;12(4): 414–419.

4. Gao YK. Improvement of fatigue property in 7050–T7451 aluminum alloy by laser peening and shot peening. *Mater Sci Eng: A.* 2011;528(10–11): 3823–3828.

5. Liu Q, Yang CH, Ding K, Barter SA, Ye L. The effect of laser power density on the fatigue life of laser-shock-peened 7050 aluminium alloy. *Fatigue Fract Eng Mater Struct.* 2007;30(11): 1110–1124.

6. Masaki K, Ochi Y, Matsumura T, Sano Y. Effects of laser peening treatment on high cycle fatigue properties of degassing-processed cast aluminum alloy. *Mater Sci Eng: A.* 2007;468-470: 171–175.

7. Sano Y, Masaki K, Gushi T, Sano T. Improvement in fatigue performance of friction stir welded A6061-T6 aluminum alloy by laser peening without coating. *Mater Des.* 2012; 36:809–814.

8. Wagner L, Mhaede M, Wollmann M, Altenberger I, Sano Y. Surface layer properties and fatigue behavior in Al 7075–T73 and Ti–6Al–4V: Comparing results after laser peening; shot peening and ball‐burnishing. *Int J Struct Integr.* 2011;2(2): 185–199.

9. Luong H, Hill MR. The effects of laser peening and shot peening on high cycle

fatigue in 7050-T7451 aluminum alloy. *Mater Sci Eng: A.* 2010;527(3): 699–707.

10. Hammond DW, Meguid SA. Crack propagation in the presence of shot-peening residual stresses. *Eng Fract Mech.* 1990;37(2): 373–387.

11. Zupanc U, Grum J. Effect of pitting corrosion on fatigue performance of shot-peened aluminium alloy 7075–T651. *J Mater Process Technol.* 2010;210(9): 1197–1202.

12. Inoue A, Sekigawa T, Oguri K, Tagawa T, Ishikawa T. Mechanism of fatigue life improvement due to fine particle shot peening in high strength aluminum alloy. *J Jpn Inst Metals.* 2010;74(6): 370–377.

13. Barter SA, Molent L. Fatigue cracking from a corrosion pit in an aircraft bulkhead. *Eng Fail Anal.* 2014;39: 155–163.

14. Takahashi K, Amano T, Ando K, Takahashi F. Improvement of fatigue limit by shot peening for high-strength steel containing a crack-like surface defect. *Int J Struct Integr.* 2011;2(3): 281–292.

15. Yasuda J, Takahashi K, Okada H. Improvement of fatigue limit by shot peening for high-strength steel containing a crack-like surface defect: Influence of stress ratio. *Int J Struct Integr.* 2014;5(1): 45–59.

16. Sakamoto J, Lee Y-S, Cheong S-K. Effect of surface flaw on fatigue strength of shot-peened medium-carbon steel. *Eng Fract Mech.* 2015;133(0): 99–111.

17. Fueki R, Takahashi K, Handa M. Fatigue limit improvement and rendering defects harmless by needle peening for high rensile steel welded joint. *Metals.* 2019;9(2): 143.

18. Cláudio RA, Silva JM, Branco CM, Byrne J. A fracture mechanics based approach to predict fatigue life of scratch damaged shot peened components. *Procedia Eng.*

2011;10: 2672–2677.

19. Takahashi K, Osedo H, Suzuki T, Fukuda S. Fatigue strength improvement of an aluminum alloy with a crack-like surface defect using shot peening and cavitation peening. *Eng Fract Mech.* 2018;193: 151–161.

20. Zhang XQ, Li H, Yu XL, et al. Investigation on effect of laser shock processing on fatigue crack initiation and its growth in aluminum alloy plate. *Mater Des.* 2015;65: 425–431.

21. Zhang L, Lu JZ, Zhang YK, et al. Effects of different shocked paths on fatigue property of 7050-T7451 aluminum alloy during two-sided laser shock processing. *Mater Des.* 2011;32(2): 480–486.

22. Tan Y, Wu G, Yang J-M, Pan T. Laser shock peening on fatigue crack growth behaviour of aluminium alloy. *Fatigue Fract Eng Mater Struct.* 2004;27(8): 649–656.

23. Chahardehi A, Brennan FP, Steuwer A. The effect of residual stresses arising from laser shock peening on fatigue crack growth. *Eng Fract Mech.* 2010;77(11): 2033–2039.

24. Smyth NA, Toparli MB, Fitzpatrick ME, Irving PE. Recovery of fatigue life using laser peening on 2024-T351 aluminium sheet containing scratch damage: The role of residual stress. *Fatigue Fract. Eng. Mater. Struct.* 2019;42(5):1161-1174

25. Spanrad S, Tong J. Characterisation of foreign object damage (FOD) and early fatigue crack growth in laser shock peened Ti–6Al–4V aerofoil specimens. *Mater. Sci. Eng. A*. 2011;528(4-5):2128-2136

26. Zabeen S, Preuss M, Withers PJ. Evolution of a laser shock peened residual stress field locally with foreign object damage and subsequent fatigue crack growth.

*Acta Materialia*. 2015;83(15):216-226

27. Masaki K, Tsuji T, Kobayashi Y. Effect of peening treatment for out-of-plane fatigue test on A7075–T651 alloy. *Trans JSME (in Japanese)*. 2015;81(826): 15–00003.

28. Society of Automotive Engineers. Residual stress measurement by X-ray diffraction-SAE J784a. Society of Automotive Engineers; 1971:64.

29. Acceptable Defect size Research Comittie. The research committee report of the acceptable defect size for spring steel. *Trans Jpn Soc Spring Eng (in Japanese).* 2008;2008(53): 57–66.

30. Newman Jr JC, Raju IS. An empirical stress-intensity factor equation for the surface crack. *Eng Fract Mech.* 1981;15(1–2): 185–192.

31. Lee EU, Glinka G, Vasudevan AK, Iyyer N, Phan ND. Fatigue of 7075–T651 aluminum alloy under constant and variable amplitude loadings. *Int J Fatigue.* 2009;31(11): 1858–1864.

32. Forth SC, Newman JC, Forman RG. On generating fatigue crack growth thresholds. *Int J Fatigue.* 2003;25(1): 9–15.

33. Fernández-Pariente I, Bagherifard S, Guagliano M, Ghelichi R. Fatigue behavior of nitrided and shot peened steel with artificial small surface defects. *Eng Fract Mech.* 2013;103(0): 2–9.

34. Zhang J, Li X, Yang B, Wang H, Zhang J. Effect of micro-shot peening on fatigue properties of precipitate strengthened Cu-Ni-Si alloy in air and in salt atmosphere. *Surf Coat Technol.* 2019;359: 16–23.

35. Kitagawa H, Takahashi S. Applicability of fracture mechanics to very small cracks or the crack in the early stage. *Proceedings of the Second International*

*Conference on Mechanical Behaviour of Material.* 1976: 627–631.

36. Smith RA, Miller KJ. Prediction of fatigue regimes in notched components. *Int J Mech Sci.* 1978;20(4): 201–206.

37. El Haddad MH, Topper TH, Smith KN. Prediction of non propagating cracks. *Eng Fracture Mech.* 1979;11(3): 573–584.